Muon-spin-rotation measurements of the London penetration depths in $YBa_2Cu_3O_{6.97}$

B. Pümpin, H. Keller, W. Kündig, W. Odermatt,* I. M. Savić,† J. W. Schneider, H. Simmler, and P. Zimmermann
Physik-Institut der Universität Zürich, CH-8001 Zürich, Switzerland

E. Kaldis and S. Rusiecki
Laboratorium für Festkörperphysik, Eidgenössische Technische Hochschule Zürich, CH-8093 Zürich, Switzerland

Y. Maeno‡ and C. Rossel
IBM Research Division, Zürich Research Laboratory, CH-8803 Rüschlikon, Switzerland

(Received 6 March 1990)

Muon-spin-rotation (μSR) experiments on a high-quality sintered $YBa_2Cu_3O_x$ sample [$x=6.970(1)$] were performed, in order to obtain an accurate knowledge of the magnitude and the temperature dependence of the magnetic penetration depth in this copper oxide superconductor. Special attention was given to the data analysis. In particular, the systematic errors introduced by different types of analyses were estimated. Our results show that the temperature dependence of the effective penetration depth λ_{eff} into the sintered sample is well described by the two-fluid model, with $\lambda_{eff}(0)=155(10)$ nm. This behavior of $\lambda_{eff}(T)$ is consistent with conventional s-wave pairing. With the anisotropy ratio $\gamma=\lambda_c/\lambda_{ab}=5(1)$ measured in a previous μSR experiment, the penetration depths $\lambda_{ab}(0)=130(10)$ nm and $\lambda_c(0)=500-800$ nm (parallel and perpendicular to the CuO_2 planes, respectively) were extracted. Our results are compared with those obtained by other experimental techniques and theoretical predictions.

I. INTRODUCTION

Due to the potential applications of superconductivity at temperatures near or above that of liquid nitrogen, a world-wide effort has been made to understand the physical properties of high-T_c superconductors. Among these copper-oxide-based materials, $YBa_2Cu_3O_x$ has been the subject of a great number of experimental and theoretical investigations. However, the nature of the pairing mechanisms and the origin of the high critical temperature are still unknown. A possible way to learn more about the microscopic behavior of $YBa_2Cu_3O_x$ is by studying one of its characteristic quantities, the magnetic penetration depth λ. In the clean limit (mean free path much greater than the coherence length) the London penetration depth is given by

$$\lambda=(m^*/\mu_0 e^2 n_s)^{1/2}\ , \tag{1}$$

where m^* is the effective mass of the superconducting carriers and n_s is the superconducting carrier density. Since n_s is closely related to the superconducting order parameter Ψ ($n_s=|\Psi|^2$), the temperature dependence of λ contains crucial information on the involved pairing mechanism (s or p wave, weak or strong coupling). In addition, the zero-temperature value $\lambda(0)$ sets a scale for the screening of an external field B_{ext}. In order to determine the magnitude of λ and its temperature dependence in the copper oxide superconductor $YBa_2Cu_3O_x$, different techniques such as muon spin rotation (μSR),[1-7] magnetization experiments,[8-12] kinetic inductance,[13] and microwave absorption[14] have been applied. However, the interpretation of the experimental data is controversial. While some groups observe a BCS-like behavior[11-13] of $\lambda(T)$, other groups report a temperature dependence which is described by the empirical two-fluid model.[1,3-7] Factors such as different sample preparation, surface effects, or macroscopic averaging can be the cause of the disagreement among the published results.

In this paper we present μSR experiments on a *high-quality* sintered $YBa_2Cu_3O_x$ sample. By applying the μSR technique to the study of superconductors, one can gain important information on the magnetic flux line structure in the *bulk* of a sample. The muon, which acts as a *microscopic* probe of the local magnetic field distribution $p(B_\mu)$, provides an elegant way to measure the London penetration depth λ. Due to the rather large sample size required for μSR measurements, most of the experiments were performed on polycrystalline sintered samples. Until now, μSR spectra were, in general, analyzed by assuming a standard Gaussian field distribution $p(B_\mu)$. As shown by Brandt,[15] this type of data analysis can lead to significant systematic errors if performed on an isotropic type-II superconductor. However, the consequences of this analysis method with respect to a polycrystalline sintered sample were never studied in detail. The motivation of this work was to determine accurately the magnitude and the temperature dependence of the penetration depths in $YBa_2Cu_3O_x$ and estimate the influence of possible systematic errors on the results. The basic principles of the μSR technique are described in Sec. II. Special attention was given to the experimental setup in order to

optimize the signal-to-noise ratio. Section III is a summary of the theory underlying this work. A precise knowledge of the second moment of the μSR frequency spectrum allows one to determine λ_{eff}, the effective magnetic penetration depth into the sintered sample. A study of the magnetic behavior of a uniaxial superconductor such as $YBa_2Cu_3O_x$ would not be complete without taking into account the anisotropy of the magnetic field distribution in the sample. Based on theoretical results of Barford and Gunn,[16] the penetration depths λ_{ab} (screening currents flowing along the crystallographic a and b axes) and λ_c (screening currents flowing along the c axis) can be calculated from λ_{eff}, provided that the strength of the anisotropy is known. The μSR measurements and the different types of fitting procedures used to extract the μSR frequency spectra are presented in Sec. IV. In Sec. V our results are discussed and compared with theoretical calculations and experimental results obtained by other techniques.

II. THE μSR TECHNIQUE

The positive muon (μ^+) is a lepton with a mass of $m_\mu \approx 207 m_e$ (electron mass m_e) and a spin $S=\frac{1}{2}$. In a μSR experiment, spin-polarized positive muons are implanted (one at a time) into a sample that is situated in an external field $\mathbf{B}_{\text{ext}}$ perpendicular to the initial polarization direction. The incoming muon is detected by a muon counter which starts a clock ($t=0$). During the thermalization process (10^{-13} s), the muon keeps its polarization and subsequently precesses in the local magnetic field B_μ (at the muon) with the Larmor frequency $\omega_\mu=\gamma_\mu B_\mu$, where $\gamma_\mu=2\pi\times 135.5$ MHz/T is the gyromagnetic ratio of the muon. The muon then decays into a positron and two neutrinos with a lifetime of 2.2 μs. Due to parity violation, the decay positron is preferentially emitted along the muon-spin direction. When registered by one of the two positron counters (arranged under 180° along the initial muon-spin polarization), the decay positron stops the clock. The observed μSR time histograms may be written in the form

$$N(t)=N_0\exp(-t/\tau_\mu)[1+AP(t)]+b \ , \tag{2}$$

where N_0 is a normalization constant, τ_μ the muon lifetime, A the maximum experimental decay asymmetry (precession amplitude), $P(t)$ the time evolution of the muon-spin polarization, and b a time-independent, uncorrelated background. In the simplest case of a homogeneous magnetic field $\mathbf{B}_\mu$, the time-dependent muon-spin polarization is given by[16,17]

$$P_x(t)=P_x(0)\frac{B_y^2+B_z^2}{B_\mu^2}\cos(\gamma_\mu B_\mu t) \ , \tag{3}$$

where x is the direction parallel to the initial muon-spin polarization $P_x(0)$, z is the direction parallel to the external field, and B_x, B_y, B_z are the components of the local field $\mathbf{B}_\mu$. For an arbitrary field distribution $p(\mathbf{B}_\mu)$, the general form of $P_x(t)$ is

$$P_x(t)=P_x(0)\int \frac{B_y^2+B_z^2}{B_\mu^2}\cos(\gamma_\mu B_\mu t)p(\mathbf{B}_\mu)d^3B \ . \tag{4}$$

The equation is only valid if the muon does not diffuse in the sample. An integration over polar coordinates leads to the expression

$$P_x(t)=P_x(0)\gamma_\mu\int_0^\infty F(\gamma_\mu B_\mu)\cos(\gamma_\mu B_\mu t)dB_\mu \ , \tag{5}$$

where $F(\gamma_\mu B_\mu)$ is a weighting factor for the signal with the precession frequency $\omega_\mu=\gamma_\mu B_\mu$. Note that in the special case where all the local magnetic fields are parallel to the applied field $\mathbf{B}_{\text{ext}}$, $F(\omega_\mu)$ is related to $p(B_\mu)$ by means of the equation

$$p(\omega_\mu/\gamma_\mu)=\gamma_\mu F(\omega_\mu) \ .$$

For a Gaussian distribution of static internal fields, $P_x(t)$ has the following simplified form:[17]

$$P_x(t)=P_x(0)\exp(-\sigma^2t^2)\cos(\gamma_\mu\langle B_\mu\rangle t) \ , \tag{6}$$

where $\langle B_\mu\rangle$ is the first moment of $p(B_\mu)$ and σ the muon depolarization rate. The second moment $\langle \Delta B_\mu^2\rangle$ of $p(B_\mu)$ can then be determined from σ by means of

$$\langle \Delta B_\mu^2\rangle=\int_0^\infty (B_\mu^2-\langle B_\mu\rangle^2)p(B_\mu)dB_\mu=2\sigma^2/\gamma_\mu^2 \ . \tag{7}$$

At this point, one should remark that a slightly different definition of σ also appears in the literature. For instance, in Refs. 3, 4, and 18, the μSR depolarization rate σ is defined by the relation $\langle \Delta B_\mu^2\rangle=\sigma^2/\gamma_\mu^2$. Therefore, the values of σ quoted in Refs. 3, 4, and 18 have to be divided by $\sqrt{2}$ for comparison with the present values of σ.

In general, the field distribution in a sample is far from Gaussian and the desired information concerning $p(B_\mu)$ has to be extracted in some other way. It will be shown in Sec. IV that $F(\omega_\mu)$, here called the μSR frequency spectrum, is obtained from the *real* part of the Fourier transform of $P_x(t)$ or by numerically solving Eq. (5). Although $F(\omega_\mu)$ is not always proportional to $p(B_\mu)$, it still contains important information on the local magnetic field distribution in the bulk of the sample and can, for instance, be compared with results from theoretical calculations.

The experiments presented in this work were performed in the $\pi M3$ area of the Paul Scherrer Institute (PSI, Switzerland) using low-momentum muons (29 MeV/c). A helium-flow cryostat allowed a temperature range between 8 and 300 K, with a stability of ± 0.1 K. A Helmholtz coil was used to apply external magnetic fields up to 380 mT. An important aspect of μSR experiments on high-T_c superconductors is to ensure that *all* the muons stop in the sample. Muons stopping in the sample holder or in the cryostat windows precess in the external field. This "correlated background" has the form of a spectral line at the frequency $\gamma_\mu B_{\text{ext}}$ and is superimposed on the signal originating in the sample. Due to the complicated shape of the field distribution in a superconductor (see Sec. III), the separation of both signals (sample and sample holder) is not straightforward and can be the source of systematic errors. A spin rotator was used to reduce the correlated background to a

minimum. With this experimental setup the external field was applied parallel to the muon momentum, focusing the particles on the sample. Although the samples had diameters between 14.5 and 25 mm, the beam was collimated to a diameter of only 8 mm in order to keep the correlated background as low as possible. In addition, the samples were mounted on a hematite (Fe_2O_3) target holder. Fe_2O_3 is an antiferromagnet and muons stopping in this material see a local field of the order of 1.6 T. The corresponding spectral line does not interfere with the signal originating from the sample. To minimize the number of muons stopping somewhere in the beam line (muon counter, cryostat windows, etc), the range of the material between the production target and the sample was reduced to about 60 mg/cm^2. With all these precautions only 5(1)% of the detected muons contributed to a correlated background signal. With the density of the samples being of the order of 5.3 g/cm^3, the low-momentum muons (range 150 mg/cm^2) stopped in a depth of approximately 280 μm. The μSR technique is therefore an important method to study the bulk properties of high-temperature superconductors.

III. VORTEX LATTICE AND MAGNETIC PENETRATION DEPTH

In the Shubnikov phase of a type-II superconductor, the external magnetic field ($B_{\rm ext} > B_{c1}$) penetrates the sample in the form of a (more or less) regular vortex lattice. For external fields $B_{\rm ext} < B_{c2}/4$, the London picture applies and the local magnetic field in an isotropic superconductor can be written as[19]

$$\mathbf{B}(\mathbf{r}) = \mathbf{B}_{\rm ext} \sum_{Q} \frac{\exp(i\mathbf{Q}\cdot\mathbf{r})}{1+\lambda^2 Q^2} , \tag{8}$$

where the Q's are the reciprocal-lattice vectors. Calculations of the expected field distributions for different values of the applied field $B_{\rm ext}$ were performed by Brandt.[15] In the case of an isotropic superconductor, the local fields are parallel to the applied field and the field distribution $p(B)$ can directly be compared to the μSR frequency spectrum. The second moment of $p(B)$ is then given by[15]

$$\langle \Delta B^2 \rangle_{\rm isotropic} = 0.003\,71 \Phi_0^2 \lambda^{-4} , \tag{9}$$

where Φ_0 is the elementary flux quantum and λ the London penetration depth. This equation is only valid for high magnetic fields ($B_{\rm ext} > 2B_{c1}$), where $\langle \Delta B^2 \rangle$ is independent of $B_{\rm ext}$.[15]

The generalization to the anisotropic case is obtained by replacing the effective mass m^* in Eq. (1) by a diagonal mass tensor $\mathbf{m}^*$.[20] In uniaxial superconductors, the tensor $\mathbf{m}^*$ has a degenerate eigenvalue m_{ab} associated with supercurrents flowing in the ab planes and an eigenvalue m_c associated with supercurrents flowing along the c axis. Consequently, the London equation (1) has a more general form

$$\lambda_{ab,c} = (m^*_{ab,c}/\mu_0 e^2 n_s)^{1/2} , \tag{10}$$

where λ_{ab} and λ_c are the penetration depths when the screening currents are flowing in the ab planes and along the c axis, respectively. Theoretical calculations[20–23] show that there are substantial differences between the magnetic field distributions in uniaxial and isotropic type-II superconductors. The two field distributions are only similar if the external field is parallel to the crystallographic c axis of the uniaxial superconductor. In this case, the local magnetic fields are parallel to $\mathbf{B}_{\rm ext}$ and the equilibrium lattice structure consists of equilateral triangles. For $\mathbf{B}_{\rm ext}$ perpendicular to the c axis, the local magnetic fields in the uniaxial superconductor are still parallel to the external field but the vortex lattice is probably distorted to isosceles triangles.[22,23] Considering these effects of anisotropy, Barford and Gunn[16] derived the following expressions for the second moment of $p(B)$:

$$\langle \Delta B^2 \rangle_{\parallel} = 0.003\,71 \Phi_0^2 \lambda_{ab}^{-4} \tag{11}$$

and

$$\langle \Delta B^2 \rangle_{\perp} = 0.003\,71 \Phi_0^2 (\sqrt{\lambda_{ab}\lambda_c})^{-4} \tag{12}$$

for $\mathbf{B}_{\rm ext} \| \mathbf{c}$ and $\mathbf{B}_{\rm ext} \perp \mathbf{c}$, respectively. Equation (12) shows that, for $\mathbf{B}_{\rm ext}$ perpendicular to the c axis, the effective penetration depth is the geometric mean of λ_{ab} and λ_c. In this geometry, the supercurrents flow in the ab planes and along the c axis[23] so that the screening of $B_{\rm ext}$ depends on λ_c as well as on λ_{ab}. An important quantity with respect to uniaxial superconductors is the anisotropy ratio γ which, according to Eq. (10), is given by

$$\gamma = (m_c^*/m_{ab}^*)^{1/2} = \lambda_c/\lambda_{ab} . \tag{13}$$

Together with Eqs. (11) and (12), we obtain the useful relation

$$\gamma = (\langle \Delta B^2 \rangle_{\parallel} / \langle \Delta B^2 \rangle_{\perp})^{1/2} . \tag{14}$$

Using single crystals, it would be possible to determine the values of λ_{ab}, λ_c, and γ directly. Unfortunately, good single crystals which are large enough for μSR experiments (at least $5\times5\times1$ mm^3) are not easy to obtain. On the other hand, sintered polycrystalline samples can nowadays be produced in large sizes and of high purity. In such samples, the observed field distribution is an average over all orientations. Note that, for an arbitrary orientation of $\mathbf{B}_{\rm ext}$ with respect to the c axis, transverse field components are present in the sample and the equilibrium lattice has a complicated structure.[20–23] To get an idea of the shape of the μSR frequency spectrum $F(\omega_\mu)$ in a sintered sample, see Refs. 24 and 25, where μSR frequency spectra were calculated under the assumption of an extreme anisotropic type-II superconductor with $\lambda_c = \infty$. Due to the components of the local field B_μ (at the muon) which are transverse to $\mathbf{B}_{\rm ext}$, the second moment of $p(B_\mu)$ cannot be calculated from our μSR data. Nevertheless, an effective penetration depth $\lambda_{\rm eff}$ can be defined by means of[16]

$$\langle \Delta\omega_\mu^2 \rangle_{\rm polycrystal} = 0.003\,71 \gamma_\mu^2 \Phi_0^2 \lambda_{\rm eff}^{-4} , \tag{15}$$

where $\langle \Delta\omega_\mu^2 \rangle$ is the second moment of the μSR frequency spectrum $F(\omega_\mu)$. As for Eqs. (9), (11), and (12), this equation is only meaningful for high magnetic fields

where $\langle \Delta\omega_\mu^2 \rangle$, or $\langle \Delta B^2 \rangle$, is independent of B_{ext}. Barford and Gunn[16] showed that, in the special case of a large anisotropy ratio ($\gamma \geq 5$), λ_{eff} is solely determined by λ_{ab}:

$$\lambda_{eff} \approx 1.23 \lambda_{ab} \ . \tag{16}$$

This equation indicates that, for a uniaxial superconductor with large anisotropy, the screening of the external field is mainly influenced by the currents flowing in the *ab* planes. Thus, λ_{ab} and λ_c can be determined from a μSR experiment on a polycrystalline sample by means of Eqs. (13) and (16) if the anisotropy ratio is known *a priori*.

So far we have neglected the influence of the temperature on the penetration depth λ_{eff}. However, Eq. (15) is valid for all $T < T_c$, and the temperature dependence of the penetration depth can answer a number of questions concerning the nature of the pairing mechanism in the superconductor. For example, the fact that $\lambda(T)$ in the heavy-fermion superconductor UBe_{13} varies as T^2 for $T/T_c \ll 1$ has been interpreted as evidence for *p*-wave superconductivity.[26] For conventional *s*-wave superconductors with the weak-coupling ratio $2\Delta_0/k_B T_c = 3.52$ (Δ_0 is the superconducting energy gap), the temperature dependence of λ is given by the mean-field BCS theory[27]

$$\lambda(T) = \lambda(0) \sqrt{1 - [\partial \ln \Delta(T) / \partial \ln T]} \ , \tag{17}$$

where $\Delta(T)$ represents the superconducting gap energy. Due to the large range of coherence lengths, penetration depths, mean free paths, or coupling strengths observed in superconductors, it is not surprising that deviations from the BCS behavior can occur. For conventional *s*-wave superconductors, the experimentally observed temperature dependence of λ is often described by the empirical two-fluid model:

$$\lambda(T) = \lambda(0) [1 - (T/T_c)^4]^{-1/2} \ . \tag{18}$$

The theoretical meaning of such a temperature dependence will be discussed in Sec. V.

At this point, one should emphasize that the equations in this section are only valid under the assumption that a vortex lattice is formed in the superconducting sample. Although several experimental[28–31] and theoretical[32,33] investigations report evidence for a glassy behavior in $YBa_2Cu_3O_x$ at temperatures near T_c, Bitter pattern experiments[34–36] show that a short-range ordered vortex lattice does exist at low temperatures. This justifies the use of Eqs. (15) and (18) at low temperatures to extrapolate the value of the magnetic penetration depth $\lambda_{eff}(0)$ in $YBa_2Cu_3O_x$.

IV. EXPERIMENTS AND RESULTS

μSR experiments were performed on two sintered nearly "equilibrium" samples of $YBa_2Cu_3O_x$ [$x = 6.970(1)$ and 6.962(1)] which were prepared at the Eidgenössische Technische Hochschule (ETH) Zurich.[37] No zirconium gettering or quenching have been used because they lead to more or less nonequilibrium samples. Instead, it was tried to come as near as possible to the thermodynamic equilibrium using long times for the solid-state reaction at 950 °C and slow cooling to room temperature. The results for both samples are essentially consistent, so that only those for $x = 6.970(1)$ will be presented in detail. The method for the accurate determination of the oxygen concentration has been described elsewhere.[38] Magnetization measurements exhibit a very sharp transition at $T_c = 89.5$ K with a width of 8 K (10–90 %) and a Meissner fraction of approximately 60% in a field of 1.42 mT (Fig. 1). The disk-shaped sample had a diameter of 14.5 mm and thickness of 3.5 mm. Its density was about $\rho \simeq 5.3$ g/cm^3. The external field was applied perpendicular to the plane of the disk, giving rise to a demagnetization factor $N \approx 0.7$. To make sure that the applied field was high enough to use Eq. (15), a field scan between 5 and 350 mT was performed (Fig. 2). Every single point of this scan was obtained after field cooling (FC) the sample from above T_c to 10 K. In a first step, the data were analyzed by performing least-square fits to the time histograms $N(t)$ given in Eq. (2), assuming a Gaussian field distribution $p(B_\mu)$ with a depolarization rate σ [see Eq. (6)]. As shown in Fig. 2, σ [which, by means of Eq. (7), is

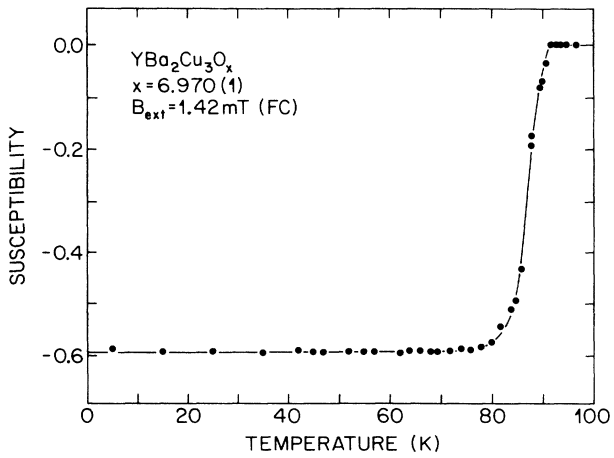

FIG. 1. Magnetic susceptibility of a sintered $YBa_2Cu_3O_x$ sample measured with a SQUID susceptometer as a function of temperature in a field of 1.42 mT (after field cooling, FC). Note the large Meissner fraction ($\approx 60\%$) and the sharp transition at $T_c = 89.5$ K.

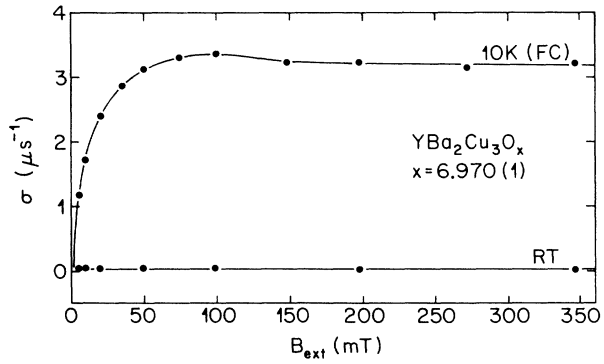

FIG. 2. Depolarization rate σ as a function of the external field B_{ext} (FC) for a sintered $YBa_2Cu_3O_x$ sample at 10 K and at room temperature (RT), respectively. The lines are guides to the eye.

proportional to $\langle \Delta B_\mu^2 \rangle^{1/2}$] increases almost linearly below 20 mT ($\leq B_{c1}$) until reaching a maximum at 100 mT. Above 150 mT, the depolarization rate is independent of the external field. For comparison, the corresponding field dependence of σ measured at room temperature (RT) is also displayed in Fig. 2. As expected, only a small and field independent $\sigma_0 \approx 0.1\ \mu s^{-1}$ is observed, arising most likely from nuclear copper moments. The maximum of $\sigma(B)$ as observed for the superconducting sample (10 K) at 100 mT can be explained by a distortion of the flux-line lattice due to pinning.[2] Such a disorder typically contributes to an enhancement of the second moment $\langle \Delta B_\mu^2 \rangle$. At higher magnetic fields, the average intervortex spacing is small compared to the penetration depth and the interaction between the flux lines tends to reduce this disorder. The fact that the "bump" in Fig. 2 is only observed for relatively low fields[2] indicates that the sample is very homogeneous and of high quality. To summarize, the behavior of $\sigma(B)$ implies that, for a determination of the London penetration depth $\lambda_{\rm eff}$, the applied field must be larger than 150 mT.

Based on these preliminary measurements, a FC temperature scan was performed in a magnetic field of 350 mT. Figure 3 shows the depolarization rate $\sigma(T)$ after subtraction of a small temperature-independent contribution ($\sigma_0 \approx 0.1\ \mu s^{-1}$) which was determined above T_c. Note that, according to Eqs. (6) and (15), $\sigma(T)$ is proportional to $\lambda_{\rm eff}^{-2}(T)$. The solid line is a fit to the data using the temperature dependence

$$\sigma(T)=\sigma(0)[1-(T/T_c)^4]$$

given by the two-fluid model [Eq. (18)] with $\sigma(0)$ and T_c as fit parameters. The inset of Fig. 3 displays the depolarization rate σ as a function of $1-(T/T_c)^4$. The agreement between our μSR data and the two-fluid model is excellent, indicating conventional s-wave pairing. The effective penetration depth $\lambda_{\rm eff}$ was calculated from the depolarization rate σ by means of Eqs. (7) and (15) and is shown in Fig. 4.

So far the μSR time histograms were analyzed by assuming a Gaussian field distribution $p(B_\mu)$. However, as mentioned in Sec. III, the field distribution in a type-II superconductor can be very complicated. A critical discussion on the consequences of fitting a Gaussian function to the local magnetic field distribution in an isotropic type-II superconductor is given in Ref. 15. The situation is somehow different in a sintered sample of a uniaxial type-II superconductor. In order to estimate the systematic error introduced by the choice of a Gaussian fitting function, two more general types of data analysis were performed, allowing a model-independent determination of the μSR frequency spectrum $F(\omega_\mu)$ and its second moment $\langle \Delta\omega_\mu^2 \rangle$. In method I, the μSR frequency spectrum $F(\omega_\mu)$ is extracted from the muon-spin polarization by performing a complex Fourier transform. In method II, Eq. (5) is solved numerically.

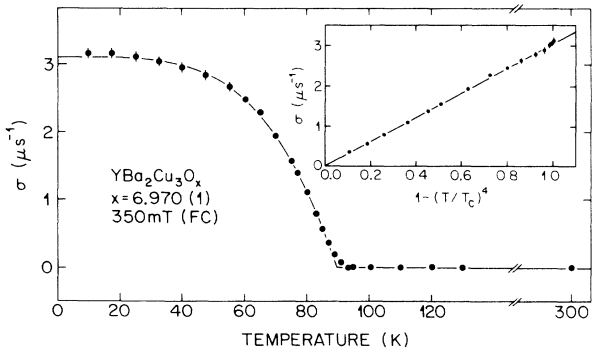

FIG. 3. Depolarization rate σ as a function of temperature for a high-quality sintered $YBa_2Cu_3O_x$ sample measured in a field of 350 mT (FC). The solid curve is a fit to the data using the empirical temperature dependence of the two-fluid model [Eq. (18)]. In the inset the same data points are plotted as a function of $1-(T/T_c)^4$.

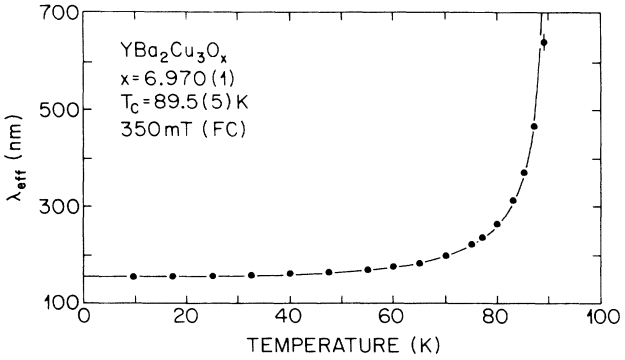

FIG. 4. Effective penetration depth $\lambda_{\rm eff}$ as a function of temperature for a high-quality sintered $YBa_2Cu_3O_x$ sample measured in a field of 350 mT (FC). The solid curve is a fit to the data using the temperature dependence of the two-fluid model [Eq. (18)].

It was shown by Brandt and Seeger[39] that, in a sample where all the local fields are parallel to the external field, the muon-spin polarization transverse to $\mathbf{B}_{\rm ext}$ can be described by the complex quantity $P_c = P_x + iP_y$, where P_x and P_y are the x and y components of the polarization. Based on Eq. (5) and Ref. 17, the complex muon-spin polarization $P_c(t)$ can then be written as

$$P_c(t)=P_c(0)\int_0^\infty F(\omega_\mu)\exp(i\omega_\mu t)d\omega_\mu\ , \tag{19}$$

where $P_c(0)=P_x(0)$ is the initial muon-spin polarization. However, for the experiment described in this paper, the geometry of the μSR apparatus allowed only the measurement of P_x and the local magnetic fields in the sintered $YBa_2Cu_3O_x$ were not necessarily parallel to $\mathbf{B}_{\rm ext}$. For these reasons, Eq. (19) must be understood as a mathematical extension of Eq. (5). Since, in a μSR experiment, the polarization is only measured for times $t_{\rm min} < t < t_{\rm max}$ and $P_c(t)=0$ for $t < t_{\rm min}$ or $t > t_{\rm max}$, the complex Fourier transform is equal to[39]

$$\begin{aligned}\tilde{P}_c(\omega_\mu)&=P_c^{-1}(0)\int_{-\infty}^{\infty}P_c(t)\exp(-i\omega_\mu t)dt \\ &=P_c^{-1}(0)\int_{t_{\rm min}}^{t_{\rm max}}P_c(t)\exp(-i\omega_\mu t)dt\ .\end{aligned} \tag{20}$$

By using Eqs. (19) and (20), the real part of $\tilde{P}_c$ may be

written as[39]

$$\mathrm{Re}[\tilde{P}_c(\omega_\mu)] = \pi F(\omega_\mu) , \tag{21}$$

where $F(\omega_\mu)$ is the weighting function defined in Eq. (5). This relation is only valid if $t_{\min} \approx 0$ and $t_{\max} \to \infty$. Thus, $F(\omega_\mu)$ is proportional to the *real* part of the complex Fourier transform of the muon-spin polarization $P_c(t)$.[39] This statement is also valid if $P_c(t)$ is replaced by the real polarization $P_x(t)$, as long as one assumes that no components of the local fields are antiparallel to $\mathbf{B}_{\mathrm{ext}}$. Although the detour over the complex plane is not necessary to extract $F(\omega_\mu)$, this derivation clearly shows that the *power* of the complex Fourier transform (which is a standard Fourier transformation used in μSR data analysis) has only a limited physical significance. To illustrate this, the Fourier transforms of two simulated muon-spin polarizations are displayed in Fig. 5. Note that the real part of the complex Fourier transform (solid circles) shows exactly the same behavior as the input frequency distribution (thick solid line). The jump in the muon-spin polarization at $t_{\min}$ produces a nonvanishing imaginary part $\mathrm{Im}[\tilde{P}_c(\omega_\mu)]$. Due to this contribution of $\mathrm{Im}[\tilde{P}_c(\omega_\mu)]$, the shape of the Fourier power can be totally different from the input frequency distribution [Fig. 5(b)]. Figure 6 shows some artifacts arising from the finite time window over which $P_c(t)$ is known. In most μSR experiments, the first few channels of a time histogram are lost, due to noise produced by "fly-through" particles. Consequently, $t_{\min}$ is different from zero and Eq. (21) is not valid anymore. The resulting difference between $\mathrm{Re}[\tilde{P}_c(\omega_\mu)]$ and $F(\omega_\mu)$ is illustrated in a computer simulation in Fig. 6(a), where $t_{\min}$ is equal to 50 ns. For the experimental results presented in this paper, $t_{\min}$ was equal to 10 ns (eight channels with 1.25 ns) and $t_{\max} \approx 4.5$ μs. Simulations performed with this value of $t_{\min}$ showed that the difference between $\mathrm{Re}[\tilde{P}_c(\omega_\mu)]$ and $F(\omega_\mu)$ is not as dramatic as in Fig. 6(a) and that the deviation in the second moment of a Gaussian curve with $\sigma \approx 3$ μs^{-1} is equal to 7%. The oscillations in Fig. 6(b) are a well-known phenomenon, appearing when the width of a spectral line is of the order of magnitude of $1/t_{\max}$.

Some typical Fourier spectra (real part of the complex Fourier transform) for two different samples taken in an external field of 350 mT at 10-K FC are displayed in Fig. 7. Figure 7(a) shows the μSR frequency spectrum $F(\omega_\mu)$ as measured in the sintered sample. The sharp peak is an

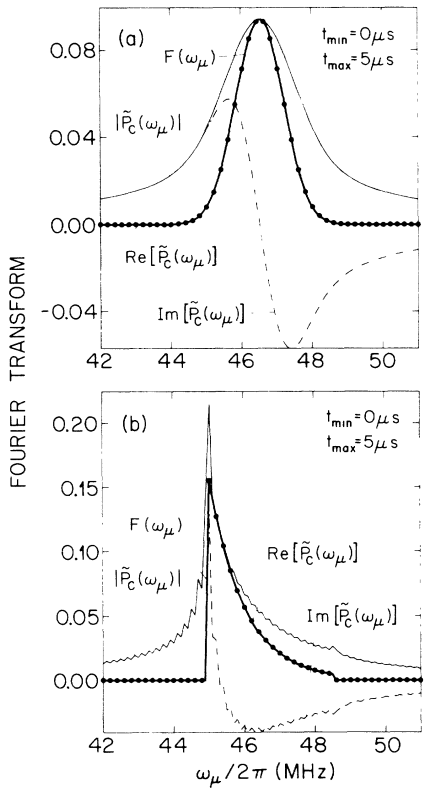

FIG. 5. Complex Fourier transforms of two simulated muon-spin polarizations $P_c(t)$. The input frequency distribution $F(\omega_\mu)$ is represented by a thick solid line. The other three spectra are proportional to the real part of the Fourier transform $\mathrm{Re}[\tilde{P}_c(\omega_\mu)]$ (solid circles), the imaginary part of the Fourier transform $\mathrm{Im}[\tilde{P}_c(\omega_\mu)]$ (dot-dashed line), and the Fourier power $|\tilde{P}_c(\omega_\mu)|$ (thin solid line). The input field distribution is (a) a Gaussian function, (b) an arbitrary frequency distribution. Note that the real part of the Fourier transform (not the power) is equal to the input frequency distribution.

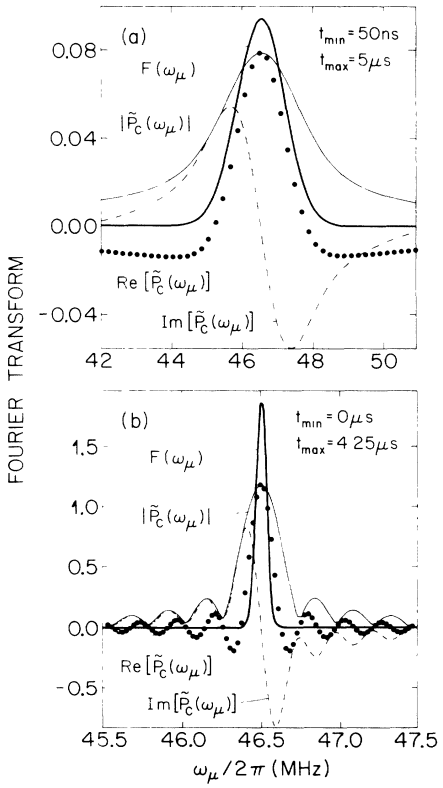

FIG. 6. Computer simulations to illustrate possible artifacts arising from a numerical Fourier transformation. The symbols follow the same convention as in Fig. 5. In (a) $t_{\min}$ is different from zero. In (b) the width of the input distribution is of the order of $1/t_{\max}$.

artifact, arising from a small fraction of the muons ($\approx 5\%$) stopping in the cryostat window and precessing in the external magnetic field. This signal corresponds to the "correlated background" described in Sec. II. Independent of this weak signal, the Fourier spectrum is slightly asymmetric, displaying a "shoulder" on the low-frequency side and a "tail" on the high-frequency side. Although the details of the spectral line are smeared out by various effects, which will be discussed in Sec. V, the results are qualitatively similar to the theoretical line shapes calculated in Refs. 24 and 25, where λ_c is assumed to be equal to infinity. The agreement between this theory and our μSR data is an indication for the strong anisotropy ratio γ present in $YBa_2Cu_3O_x$. The field distribution in the sintered sample with large γ seems to be mainly influenced by the currents flowing in the CuO_2 planes (ab planes) and almost independent of λ_c. This result is consistent with calculations by Barford and Gunn[16] [see Eq. (16)]. The data of Figs. 7(b) and 7(c) were taken on a c-axis oriented polycrystalline $YBa_2Cu_3O_x$ sample ($x \approx 6.9$) and are presented in Refs. 6 and 7. The shape of $F(\omega_\mu)$, which in this case is directly proportional to $p(B_\mu)$, shows characteristic features of the magnetic flux distribution for an Abrikosov lattice

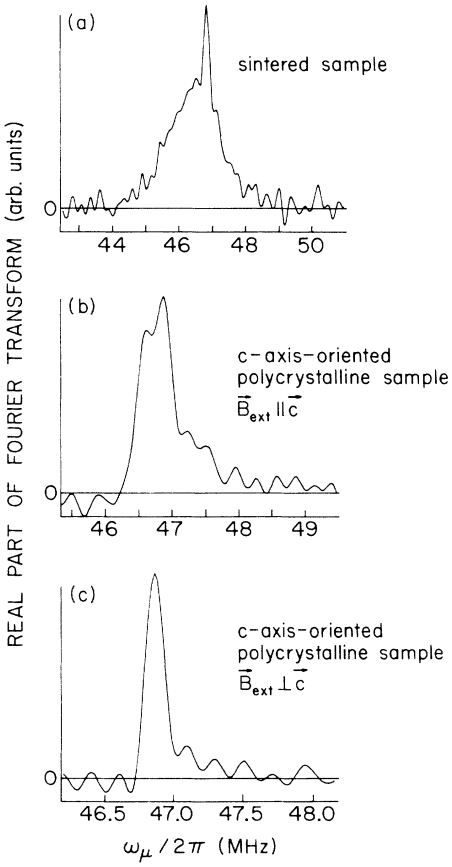

FIG. 7. Fourier spectra (real part of complex Fourier transform) of μSR time histograms taken on two $YBa_2Cu_3O_x$ samples in an external field of 350 mT (FC) at 10 K: (a) high-quality sintered sample (average over all orientations), (b) c-axis oriented crystal ($\mathbf{B}_{ext} \| \mathbf{c}$), (c) c-axis oriented crystal ($\mathbf{B}_{ext} \perp \mathbf{c}$). See also Refs. 6 and 7.

and is qualitatively in good agreement with Ref. 15. Note that the powder-averaged frequency spectrum [Fig. 7(a)] for a uniaxial superconductor is considerably more symmetric than when the external magnetic field is parallel [Fig. 7(b)] or perpendicular [Fig. 7(c)] to the c axis. This confirms our previous assumption that $F(\omega_\mu)$ in the sintered sample can be approximated by a Gaussian distribution.

A second method to obtain a model-independent value of $\langle \Delta\omega_\mu^2 \rangle$ consists of solving the integral in Eq. (5) numerically. The frequency distribution

$$F(\omega_\mu) = \sum_j a_j \cos(\gamma_\mu B_j t + \phi) ,$$

with variable amplitudes a_j and constant values of B_j and ϕ was fitted to the measured muon-spin polarization.[40] The step between two consecutive values of B_j was typically equal to 1 mT, which corresponds to the resolution determined by the finite time window of a μSR spectrum. The span between the minimal and the maximal value of B_j was chosen large enough to ensure that all the nonzero parts of the μSR frequency spectrum were within the range of the fitting frequencies.

As an example, the same μSR time spectrum (in this case at 350 mT, 10-K FC) was analyzed (a) by performing a least-squares fit to the time histogram assuming a Gaussian field distribution, (b) by taking into account the muons stopping in the cryostat window and fitting a superposition of two Gaussian lines, (c) by calculating the real part of the complex Fourier transform of the muon polarization, and (d) by numerically solving Eq. (5). The frequency spectra $F(\omega_\mu)$ obtained with the four different analysis methods are displayed in Fig. 8. The corresponding values of the square root of the second moment

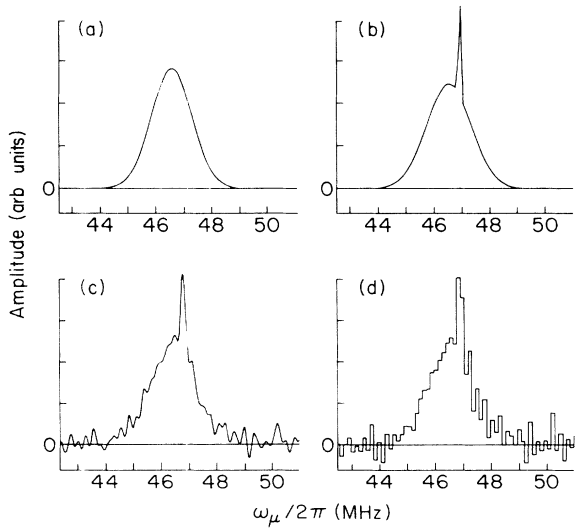

FIG. 8. Frequency spectra $F(\omega_\mu)$ obtained from the same μSR time spectrum (10-K FC, 350 mT) by using different types of data analysis: (a) Gaussian field distribution, (b) superposition of two Gaussian distributions, (c) real part of the complex Fourier transform, (d) numerical solution of Eq. (5). See also, Table I for the corresponding values of the second moment $\langle \Delta\omega_\mu^2 \rangle$.

TABLE I. Results obtained by analyzing the *same* μSR time spectrum (10-K FC, 350 mT) with four different methods (for a detailed explanation see text and Fig. 8).

Analysis method	$\langle \Delta\omega_\mu^2 \rangle^{1/2}$ (μs^{-1})	λ_{eff} (nm)
(a) Gaussian fit with one line	4.56(08)	1532(14)
(b) Gaussian fit with two lines	5.01(10)	1464(14)
(c) Real part of complex Fourier transform	4.64(15)	1521(25)
(d) Numerical solution of Eq. (5)	5.12(71)	1447(100)

of $F(\omega_\mu)$ are listed in Table I. As expected, the spectra obtained with methods (c) and (d) are almost identical. This indicates that numerical artifacts, if present, play only a minor role. The deviations from the mean value of $\langle \Delta\omega_\mu^2 \rangle^{1/2}$ lie between 4 and 7 %. Figure 8 and Table I show that the local magnetic field distribution in a sintered, unoriented $YBa_2Cu_3O_x$ [$x=6.970(1)$] sample is relatively well approximated by a Gaussian distribution. However, one must keep in mind that the systematic errors introduced by the corresponding analysis method are certainly bigger than the calculated statistic errors.

The four methods (a)–(d) described above were applied to analyze all the measured points, provided the corresponding fits converged. This means that all the μSR time spectra were analyzed with methods (a) and (b), while only the range between 10 and 87 K (10 and 65 K) was analyzed with the method (c) [method (d)]. For each method, the effective penetration depth $\lambda_{eff}(T)$ deduced from Eq. (15) was extrapolated to $T=0$ K by using the temperature dependence of the two-fluid model [Eq. (18)]. As a result of this procedure, a weighted average of $\lambda_{eff}(0)=155(10)$ nm was obtained. The error, which is mainly due to systematic effects, was estimated from the deviations between the four analysis methods.

V. DISCUSSION

The value of the anisotropy ratio γ [see Eq. (13)] in $YBa_2Cu_3O_x$ has been measured with μSR experiments,[5–7] dc magnetization,[10–12] Bitter pattern decoration experiments,[36] and torque measurements.[41,42] For comparison, an incomplete list of values of γ measured with various experimental techniques is given in Table II. For the rest of this paper, we will assume that the anisotropy ratio in $YBa_2Cu_3O_x$ is equal to $\gamma=5(1)$, as measured in a previous μSR experiment by our group.[6,7] By means of Eqs. (13) and (16), we then obtain $\lambda_{ab}(0)=130(10)$ nm and $\lambda_c(0)\approx 500-800$ nm, which are in good agreement with the values obtained with other experimental techniques on different types of samples (see Table II). Moreover, the present experimental values for $\lambda_{ab}(0)$ and $\lambda_c(0)$ agree well with the theoretical values calculated by Schneider and Frick.[43] Their results were obtained by using a BCS-type tight-binding model with an anisotropic energy gap, as observed by tunneling[44] and infrared reflectivity.[45]

Note that the values of the penetration depth obtained from μSR experiments should be regarded as lower limits. Field inhomogeneities other than those due to the regular vortex lattice can cause a broadening of the observed μSR frequency spectrum which will result in a systematic error in the calculated value of λ_{eff}. One obvious source for an unwanted line broadening is flux pinning.[15,46] Due to the small coherence lengths in $YBa_2Cu_3O_x$, the flux lines are pinned at point defects, twin planes, and grain boundaries.[35,47] However, the constant behavior of the depolarization rate σ above 150 mT (Fig. 2) seems to indicate that the pinning effects are

TABLE II. Values of the penetration depths $\lambda_{ab}(0)$, $\lambda_c(0)$, and the anisotropy ratio $\gamma=\lambda_c(0)/\lambda_{ab}(0)$ for Y-Ba-Cu-O measured by various experimental techniques. $\lambda(T)$ indicates whether the temperature dependence of the penetration depth (over the whole temperature range) is in better agreement with weak-coupling BCS theory (BCS), the two-fluid model (TF), or any other model (other). Samples: sintered sample (S), *c*-axis oriented polycrystalline sample (OP), single crystal (SC), *c*-axis oriented film (OF).

Method (sample)	$\lambda_{ab}(0)$ (nm)	$\lambda_c(0)$ (nm)	γ	$\lambda(T)$	References
μSR (S/OP)	130(10)	500–800	5(1)	TF	This work, Refs. 6, 7
μSR (OP)	146			TF	Ref. 4
μSR (SC)	141.5(3.0)	>700	>5	TF	Ref. 5
Bitter decoration (SC)			5.5(1.0)		Ref. 36
Magnetic torque (SC)	68(20)	500(70)	≈ 7		Ref. 41
Magnetic torque (OP)			4–5		Ref. 42
Magnetization (SC)	140(50)			TF[a]	Ref. 8
Magnetization (SC)	130	450	3		Ref. 10
Magnetization (OP)	130–170	640–850	5	BCS	Ref. 11
Magnetization (OP)	140(20)	610(100)	≈ 4.5	BCS	Ref. 12
Kinetic inductance (OF)	150			BCS	Ref. 13
Microwave absorption (SC)		>420		other[b]	Ref. 14

[a]For comments on the data analysis, see Ref. 9.

[b]The temperature dependence observed with this method obeys the law $\lambda(T)=\lambda(0)[2(1-T/T_c)]^{-1/2}$.

unlikely to be the cause of a strong enhancement of the second moment $\langle \Delta\omega_\mu^2 \rangle$. In addition, demagnetization effects in a polycrystalline sample due to the irregularly shaped and sized grains could also be the cause of line broadening.[18] These effects may be strong in a loose powder sample, but it is probable that, for a densely sintered sample, only the demagnetization of the whole sample plays an important role, resulting in a shift but not a broadening of the spectral line.[48,49] More theoretical work on this topic has to be done. Note that a misinterpretation of $\langle \Delta\omega_\mu^2 \rangle$ by 25% would change the resulting value of the penetration depth by only 7%. We conclude that, although the effects mentioned above are certainly present, their influence on $\lambda_{\rm eff}(0)$ is rather small. Thus, the exact value of the penetration depth most probably lies within the given error bars.

Independent of the absolute value of $\lambda_{\rm eff}(0)$, the temperature dependence of the penetration depth yields important information on the coupling mechanisms involved in $YBa_2Cu_3O_x$. A comparison of various theoretical models with our experimental results is shown in Fig. 9, where the quantity $\lambda^2(0)/\lambda^2(T)$ is displayed as a function of the reduced temperature T/T_c. The solid circles correspond to the normalized depolarization rate $\sigma(T)/\sigma(0)$ which, according to Eqs. (7), (15), and (16), is equal to $\lambda_{ab}^2(0)/\lambda_{ab}^2(T)$. As mentioned earlier (see Figs. 3 and 4), the temperature dependence of our experimental data is well described by the empirical two-fluid model (solid line). The dot-dashed and dashed curves are from Rammer[50] and describe the behavior of an s-wave superconductor with weak and strong electron-phonon coupling (clean and dirty limits), respectively. Note that, in the literature, the weak-coupling clean limit[27] is often denoted as conventional BCS behavior.[12–14] In the weak-coupling limit, the superconducting energy gap Δ_0 is related to the critical temperature T_c as $2\Delta_0/k_BT_c=3.52$. Superconductors with $2\Delta_0/k_BT_c > 3.52$ belong to the strong-coupling limit. As shown in Ref. 51, the weak- and strong-coupling limits can also be characterized by means of the parameter $k_BT_c/\hbar\omega$, where $\hbar\omega$ is a typical energy associated with the electron-phonon spectral density. Within this notation, the weak-coupling limit corresponds to the case where $k_BT_c/\hbar\omega \sim 0$, while the strong-coupling limit corresponds to $k_BT_c/\hbar\omega \leq 0.25$.[51] In order to calculate the temperature variation of the penetration depth in the strong-coupling limit, Rammer applied the Eliashberg theory for a specific model of electron-phonon spectral density.[50] Since strong-coupling effects are not very sensitive to the shape of the spectral density,[50,51] the dashed curves in Fig. 9 are representative of a whole class of similar spectral functions. Note that the Eliashberg theory was originally derived and used to describe electron-phonon coupling. Nevertheless, Blezius *et al.*[51] argue that, in a first approximation, it should be possible to apply the same theory to investigate the behavior of superconductors based on other boson-exchange mechanisms. The dotted curve in Fig. 9 was calculated by Schneider and Frick[43] and illustrates the influence of an anisotropic gap on the temperature behavior of a conventional BCS superconductor. For small values of the gap anisotropy, the temperature dependence of the penetration depth does not differ markedly from the behavior observed in the isotropic BCS limit (lower dot-dashed curve in Fig. 9). Schneider and Frick[43] found that the quantity $\lambda^2(0)/\lambda^2(T)$ decreases with increasing anisotropy and that substantial deviations from the isotropic case (see, for instance, the dotted line in Fig. 9) require the proximity to nodes in the temperature-dependent gap. As displayed in Fig. 9, none of the theories discussed above provides an absolutely satisfying description of our experimental data. Nevertheless, it has been shown by Rammer[50] that the empirical two-fluid model [Eq. (18)] gives an approximation of $\lambda(T)$ for a local ($\xi \ll \lambda$) s-wave superconductor with strong coupling. Our experimental results are thus consistent with strong-coupling s-wave pairing (see Fig. 9). Note that the temperature dependence of our data differs significantly from the behavior expected for a weak-coupling s-wave superconductor with isotropic or anisotropic gaps. One should, however, mention that the analysis performed by Schneider and Frick was restricted to systems with only one CuO_2 layer (and no CuO chain) per unit cell.[43] Therefore, the results presented in this paper should not be used to rule out the possibility of an anisotropic gap in $YBa_2Cu_3O_x$.

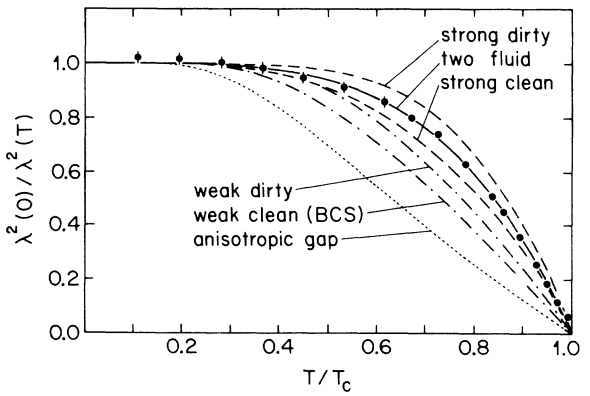

FIG. 9. Temperature dependence of $\lambda(0)^2/\lambda(T)^2[=\sigma(T)/\sigma(0)]$. The solid circles correspond to the experimental data presented in this paper. Various theoretical temperature dependences of the magnetic penetration depth are shown for comparison: weak-coupling (Refs. 26 and 50), strong-coupling (Ref. 50), tight-binding BCS model with anisotropic gap (Ref. 42), and two-fluid model (figure after Ref. 48).

It is striking that most of the μSR experiments performed on $YBa_2Cu_3O_x$ show a temperature dependence of λ which is well described by the two-fluid model.[1,3–7] On the other hand, kinetic inductance[13] and magnetization experiments[11,12] report a BCS-like behavior of the penetration depth. At this point, however, one should remark that magnetization experiments cannot always determine $\lambda(T)$ unambiguously.[8,9] These contradictory results indicate that a measurement of the temperature dependence of the magnetic penetration depth is very sensitive to systematic errors. An important advantage of μSR experiments in this context is that the muon is a *microscopic* probe of the local magnetic field in the *bulk* of the sample. In order to reach a better understanding of the temperature dependence of the penetration depth,

more experimental work must be performed on oxygen deficient $YBa_2Cu_3O_x$ $(6.4<x<7.0)$ and on other perovskite superconductors. It is, for instance, possible that the CuO chains, which are present in $YBa_2Cu_3O_7$, have an influence on the coupling strength between superconducting charge carriers. In fact, μSR experiments performed on Bi-Sr-Ca-Cu-O (a high-T_c superconductor without CuO chains) show a temperature dependence of $\lambda(T)$ consistent with weak-coupling s-wave superconductivity (with isotropic or anisotropic gap).[52] A systematic analysis of the changes in $\lambda(T)$ as a function of the oxygen concentration x in $YBa_2Cu_3O_x$ may be helpful in answering a number of questions.

In conclusion, μSR experiments were performed on a high-quality sintered $YBa_2Cu_3O_x$ sample $[x=6.970(1)]$. Special attention was given to the experimental setup and to the data analysis, in order to reduce systematic errors to a minimum. The observed μSR frequency spectra are in good agreement with theoretical calculations assuming the existence of a vortex lattice in the bulk of the superconductor.[15,24,25] From the second moment of these spectra, the effective penetration depth λ_{eff} was determined. It was found that $\lambda_{\text{eff}}(T)$ is well described by the empirical expression of the two-fluid model with $\lambda_{\text{eff}}(0)=155(10)$ nm. This observation is consistent with s-wave pairing and suggests evidence for strong coupling. From the anisotropy ratio $\gamma=5(1)$ measured in a previous μSR experiment[6,7] and the present value of $\lambda_{\text{eff}}(0)$, $\lambda_{ab}(0)=130(10)$ nm, and $\lambda_c(0)=500-800$ nm were estimated. These values are in good agreement with results obtained by other experimental techniques on different types of samples (Table II).

ACKNOWLEDGMENTS

We are very grateful to K. A. Müller, E. H. Brandt, and T. Schneider for the helpful discussions leading to this work. We would also like to thank T. Schneider and J. Rammer for allowing us to display their theoretical results in Fig. 9. Also, we wish to thank the staff of the Paul Scherrer Institute for technical assistance. This work was supported by the Swiss National Science Foundation.

*Present address: Glauser, Studer, Stüssi AG, 8032 Zurich, Switzerland.

†Present address: Faculty of Physics, University of Belgrade, 11001 Belgrade, Yugoslavia.

‡Present address: Department of Physics, Faculty of Science, Hiroshima University, Hiroshima 730, Japan.

[1]D. R. Harshman, G. Aeppli, E. J. Ansaldo, B. Batlogg, J. H. Brewer, J. F. Carolan, R. J. Cava, M. Celio, A. C. D. Chaklader, W. N. Hardy, S. R. Kreitzman, G. M. Luke, D. R. Noakes, and M. Senba, Phys. Rev. B **36**, 2386 (1987).

[2]R. F. Kiefl, T. M. Riseman, G. Aeppli, E. J. Ansaldo, J. F. Carolan, R. J. Cava, W. N. Hardy, D. R. Harshman, N. Kaplan, J. R. Kempton, S. R. Kreitzman, G. M. Luke, B. X. Yang, and D. Ll. Williams, Physica C **153-155**, 757 (1988).

[3]Y. J. Uemura, V. J. Emery, A. R. Moodenbaugh, M. Suenaga, D. C. Johnston, A. J. Jacobson, J. T. Lewandowski, J. H. Brewer, R. F. Kiefl, S. R. Kreitzman, G. M. Luke, T. Riseman, C. E. Stronach, W. J. Kossler, J. R. Kempton, X. H. Yu, D. Opie, and H. E. Schone, Phys. Rev. B **39**, 909 (1988).

[4]Y. J. Uemura, B. J. Sternlieb, D. E. Cox, V. J. Emery, A. Moodenbaugh, M. Suenaga, J. H. Brewer, J. F. Carolan, W. Hardy, R. Kadono, J. R. Kempton, R. F Kiefl, S. R. Kreitzman, G. M. Luke, P. Mulhern, T. Riseman, D. L. Williams, B. X. Yang, W. J. Kossler, X. H. Yu, H. Schone, C. E. Stronach, J. Gopalakrishnan, M. A. Subramanian, A. W. Sleight, H. Hart, K. W. Lay, H. Takagi, S. Uchida, Y. Hidaka, T. Murakami, S. Etemad, P. Barboux, D. Keane, V. Lee, and D. C. Johnston, J. Phys. (Paris) Colloq. **49**, C8-2087 (1988).

[5]D. R. Harshman, L. F. Schneemeyer, J. V. Waszczak, G. Aeppli, R. J. Cava, B. Batlogg, L. W. Rupp, E. J. Ansaldo, and D. Ll. Willams, Phys. Rev. B **39**, 851 (1989).

[6]B. Pümpin, H. Keller, W. Kündig, W. Odermatt, I. M. Savić, J. W. Schneider, H. Simmler, P. Zimmermann, J. G. Bednorz, Y. Maeno, K. A. Müller, C. Rossel, E. Kaldis, S. Rusiecki, W. Assmus, and J. Kowalewski, Physica C **162-164**, 151 (1989).

[7]H. Keller, in *Earlier and Recent Aspects of Superconductivity*, Vol. 90 of *Springer Series in Solid-State Sciences*, edited by J. G. Bednorz and K. A. Müller (Springer-Verlag, Berlin, 1990), pp. 222–239.

[8]L. Krusin-Elbaum, R. L. Greene, F. Holtzberg, A. P. Malozemoff, and Y. Yeshurun, Phys. Rev. Lett. **62**, 217 (1989).

[9]A. F. Hebard, A. T. Fiory, and D. R. Harshman, Phys. Rev. Lett. **62**, 2885 (1989); R. L. Greene, L. Krusin-Elbaum, and A. P. Malozemoff, Phys. Rev. Lett. **62**, 2886 (1989).

[10]L. Krusin-Elbaum, A. P. Malozemoff, Y. Yeshurun, D. C. Cronemeyer, and F. Holtzberg, Phys. Rev. B **39**, 2936 (1989).

[11]S. Mitra, J. H. Cho, W. C. Lee, D. C. Johnston, and V. G. Kogan, Phys. Rev. B **40**, 2674 (1989).

[12]E.-W. Scheidt, C. Hucho, K. Lüders, and V. Müller, Solid State Commun. **71**, 505 (1989).

[13]A. T. Fiory, A. F. Hebard, P. M. Mankiewich, and R. E. Howard, Phys. Rev. Lett. **61**, 1419 (1988).

[14]K. W. Blazey, Phys. Scr. **T29**, 92 (1989).

[15]E. H. Brandt, Phys. Rev. B **37**, 2349 (1988).

[16]W. Barford and J. M. F. Gunn, Physica C **156**, 515 (1988).

[17]A. Schenck, *Muon Spin Rotation Spectroscopy: Principles and Applications in Solid State Physics* (Hilger, Bristol, 1985), p. 19.

[18]Y. J. Uemura, G. M. Luke, B. J. Sternlieb, J. H. Brewer, J. F. Carolan, W. N. Hardy, R. Kadono, J. R. Kempton, R. F. Kiefl, S. R. Kreitzman, P. Mulhern, T. M. Riseman, D. Ll, Williams, B. X. Yang, S. Uchida, H. Takagi, J. Gopalakrishnan, A. W. Sleight, M. A. Subramanian, C. L. Chien, M. Z. Cieplak, Gang Xiao, V. Y. Lee, B. W. Statt, C. E. Stronach, W. J. Kossler, and X. H. Yu, Phys. Lett. **62**, 2317 (1989), and references therein.

[19]M. Tinkham, *Introduction to Superconductivity* (McGraw-Hill, New York, 1975).

[20]V. G. Kogan, Phys. Rev. B **24**, 1572 (1981).

[21]N. Schopohl and A. Baratoff, Physica C **153-155**, 689 (1988).

[22]L. J. Campbell, M. M. Doria, and V. G. Kogan, Phys. Rev. B

38, 2439 (1988).
[23]S. L. Thiemann, Z. Radović, and V. G. Kogan, Phys. Rev. B **39**, 11 409 (1989).
[24]M. Celio, T. M. Riseman, R. F. Kiefl, J. H. Brewer, and W. J. Kossler, Physica C **153-155**, 753 (1988).
[25]T. M. Riseman, Masters thesis, University of British Columbia, 1989; T. M. Riseman, J. H. Brewer, B. R. Cyca, J. F. Carolan, W. N. Hardy, R. F. Kiefl, M. Celio, W. J. Kossler, Y. J. Uemura, G. M. Luke, B. J. Sternlieb, H. Hart, K. W. Kay, H. Kojima, I. Tanaka, and K. Kakurai, Physica C **162-164**, 1555 (1989).
[26]F. Gross, B. S. Chandrasekhar, D. Einzel, K. Andres, P. J. Hirschfeld, H. R. Ott, J. Beuers, Z. Fisk, and J. L. Smith, Z. Phys. B **64**, 175 (1986).
[27]B. Mühlschlegel, Z. Phys. **155**, 313 (1959).
[28]K. A. Müller, M. Takashige, and J. G. Bednorz, Phys. Rev. Lett. **58**, 1143 (1987).
[29]B. Pümpin, H. Keller, W. Kündig, W. Odermatt, B. D. Patterson, J. W. Schneider, H. Simmler, S. Connell, K. A. Müller, J. G. Bednorz, K. W. Blazey, I. Morgenstern, C. Rossel, and I. M. Savić, Z. Phys. B **72**, 175 (1988); H. Keller, B. Pümpin, W. Kündig, W. Odermatt, B. D. Patterson, J. W. Schneider, H. Simmler, S. Connell, K. A. Müller, J. G. Bednorz, K. W. Blazey, I. Morgenstern, C. Rossel, and I. M. Savić, Physica C **153-155**, 71 (1988).
[30]P. L. Gammel, L. F. Schneemeyer, J. V. Waszczak, and D. J. Bishop, Phys. Rev. Lett. **61**, 1666 (1988).
[31]C. Rossel, Y. Maeno, and I. Morgenstern, Phys. Rev. Lett. **62**, 681 (1989).
[32]I. Morgenstern, K. A. Müller, and J. G. Bednorz, Z. Phys. B **69**, 33 (1987).
[33]M. P. A. Fisher, Phys. Rev. Lett. **62**, 1415 (1989).
[34]P. L. Gammel, D. J. Bishop, G. J. Dolan, J. R. Kwo, C. A. Murray, L. F. Schneemeyer, and J. V. Waszczak, Phys. Rev. Lett. **59**, 2592 (1987).
[35]G. J. Dolan, G. V. Chandrashekhar, T. R. Dinger, C. Feild, and F. Holtzberg, Phys. Rev. Lett. **62**, 827 (1989).
[36]G. J. Dolan, F. Holtzberg, C. Feild, and T. R. Dinger, Phys. Rev. Lett. **62**, 2184 (1989).
[37]S. Rusiecki, B. Bucher, E. Kaldis, E. Jilek, J. Karpinski, C. Rossel, B. Pümpin, H. Keller, W. Kündig, G. van Tendeloo, T. Krekels, and C. Amelinckx, *Proceedings of the E-MRS Spring Conference, Strasbourg, 1990* (Elsevier, Amsterdam, in press).
[38]K. Conder, S. Rusiecki, and E. Kaldis, Mater. Res. Bull. **24**, 581 (1989).
[39]E. H. Brandt and A. Seeger, Adv. Phys. **35**, 189 (1986).
[40]J. Hesse and A. Rübartsch, J. Phys. E **7**, 526 (1974).
[41]L. Fruchter, C. Giovannella, G. Collin, and I. A. Campbell, Physica C **156**, 69 (1988).
[42]D. E. Farrell, C. M. Williams, S. A. Wolf, N. P. Bansal, and V. G. Kogan, Phys. Rev. Lett. **61**, 2805 (1988).
[43]T. Schneider and M. Frick, in *Earlier and Recent Aspects of Superconductivity,* Vol. 90 of *Springer Series in Soild-State Sciences* (Ref. 7), pp. 501–517.
[44]J. S. Tsai, I. Takeuchi, J. Fujita, T. Yoshitake, S. Miura, S. Tanaka, T. Terashima, Y. Bando, K. Iijima, and K. Yamamoto, Physica C **153-155**, 1385 (1988).
[45]R. T. Collins, Z. Schlesinger, F. Holtzberg, and C. Feild, Phys. Rev. Lett. **63**, 422 (1989).
[46]E. H. Brandt, J. Low. Temp. Phys. **73**, 355 (1988).
[47]P. Chaudhari, Jpn. J. Appl. Phys. **26**, 2023 (1987).
[48]D. Rossier and D. E. MacLaughlin, Phys. Kondens. Mater. **11**, 66 (1970).
[49]S. Senoussi, S. Hadjoudj, R. Maury, and A. Fert, Physica C **165**, 364 (1990).
[50]J. Rammer, Europhys. Lett. **5**, 77 (1988).
[51]J. Blezius, R. Akis, F. Marsiglio, and J. P. Carbotte, Phys. Rev. B **38**, 179 (1988).
[52]H. Keller, W. Kündig, B. Pümpin, I. M. Savić, J. W. Schneider, H. Simmler, P. Zimmermann Y. Maeno, C. Rossel (unpublished); T. Schneider and M. P. Sörensen, Z. Phys. B (to be published).